SAND2022-15464C

Sandia National Laboratories

Exceptional service in the national interest

Testing and Design of Discriminants for Local Seismic Events Recorded During the Redmond Salt Mine Monitoring Experiment in Utah

Rigobert Tibi[1], Nathan Downey[1], and Ronald Brogan[2]

[1)] Sandia National Laboratories

[2)] ENSCO, Inc.

AGU Fall Meeting

12-16 December 2022

Poster S51C-03

SAND2022-

Sandia National Laboratories is a multimission laboratory managed and operated by National Technology and Engineering Solutions of Sandia LLC, a wholly owned subsidiary of Honeywell International Inc. for the U.S. Department of Energy's National Nuclear Security Administration under contract DE-NA0003525. This research was funded by the National Nuclear Security Administration, Defense Nuclear Nonproliferation Research and Development (NNSA DNN R&D). The authors acknowledge important interdisciplinary collaboration with scientists from LANL, LLNL, MSTS, PNNL, and SNL.

BACKGROUND

The Redmond Salt Mine Monitoring Experiment in Utah was designed to record seismoacoustic data at distances less than 50 km for algorithm testing and development. During the experiment from October 2017 to July 2019, six broadband seismic stations were operating at a time, with three of them having fixed locations for the duration, while the three other stations were moved to different locations every one-and-half to two-and-half months. Redmond Salt Mine operations consist of night-time underground blasting several times per week. These blasts occur in a large underground tunnel complex, tens of miles long. Redmond Mine is located within a belt of active seismicity, allowing for easy comparison of natural and anthropogenic sources.

THE REDMOND SALT MINE MONITORING EXPERIMENT

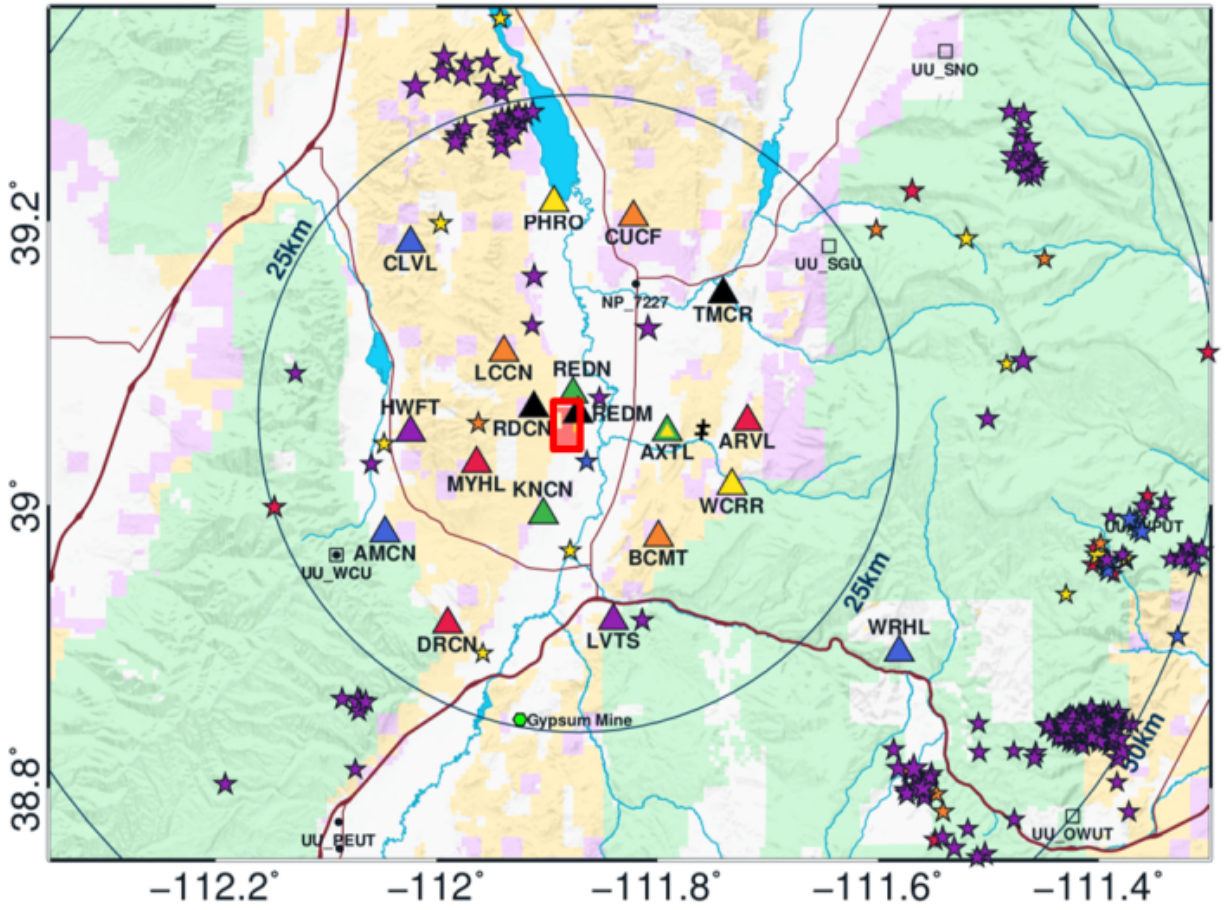

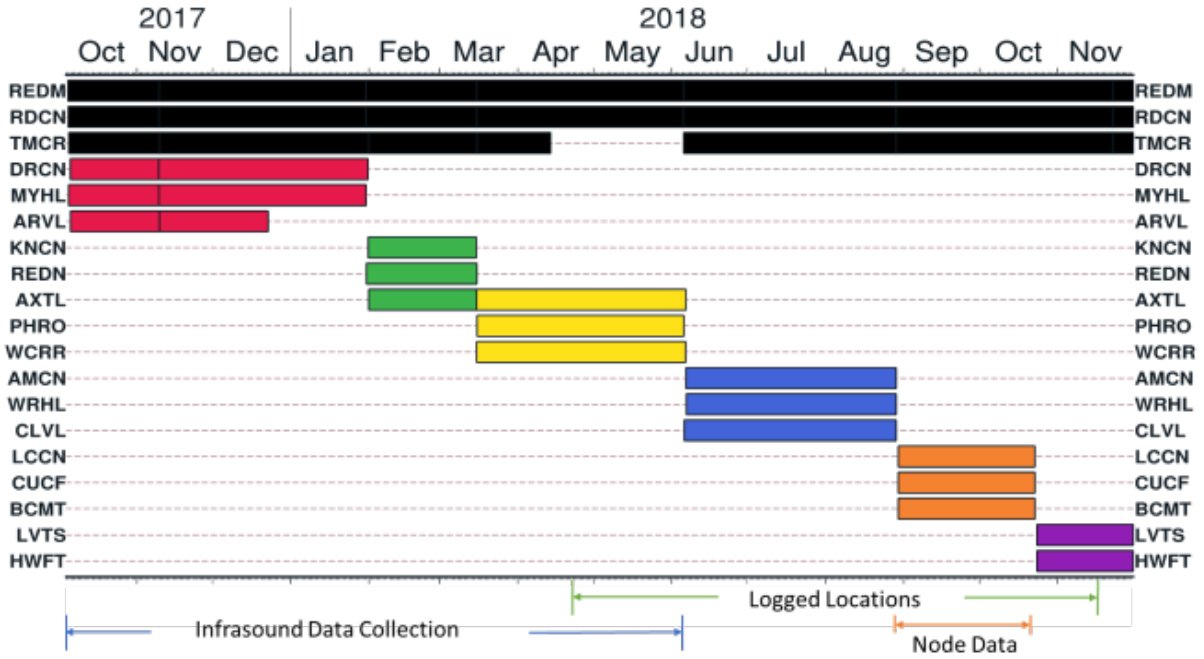

Fig. 1. (Left) Locations (triangles) of broadband stations for the Redmond Mine Experiment. The red box outlines the Redmond Mine area. (Right) Operational timeline of the stations.

DATA

Using the recorded dataset, we built 1373 events with local magnitude (M_L) of –2.4 and lower to 3.3. For 284 of the events, both M_L and the coda duration magnitude (M_C) are well constrained (see Fig. 2 on the right). Based on the event locations and the signal onset characters, this subset was divided into three populations:

- 75 blasts from the Redmond Salt Mine (**RMEs**),
- 206 tectonic earthquakes (**EQs**), and
- 3 blasts (**QBs**) from a mine/quarry located about 8 km from the Redmond Salt Mine.

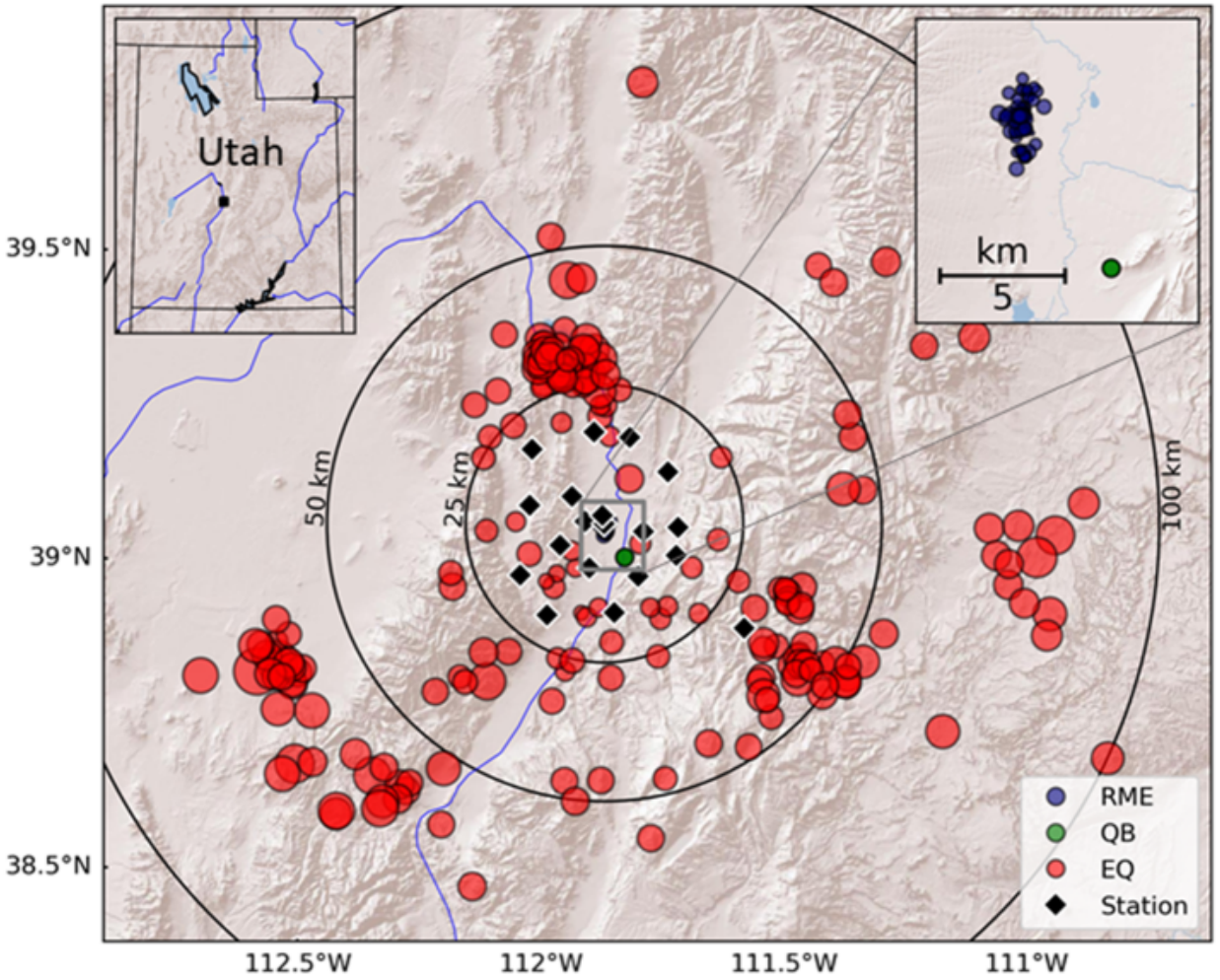

Fig. 2. Locations (circles) of the 284 events from the subset. The size of the circle is proportional to the event magnitude. Red symbols represent earthquakes (EQs), navy circles in the inset the Redmond mine events (RMEs), and green circles in the inset the quarry blasts (QBs).

We used the subset of events to design and test discriminants that are effective at local distances.

MAGNITUDE-BASED DISCRIMINATION

- For M_L calculation, the mean peak *Sg* amplitudes were estimated from the horizontal components after conversion to displacement as would be measured by a Wood-Anderson seismometer; and the empirical distance corrections were estimated according to Pechmann et al. (2007).
- M_C was calculated according to the procedure described in Pechmann et al. (2006), using the equation for the Utah region proposed by these authors.

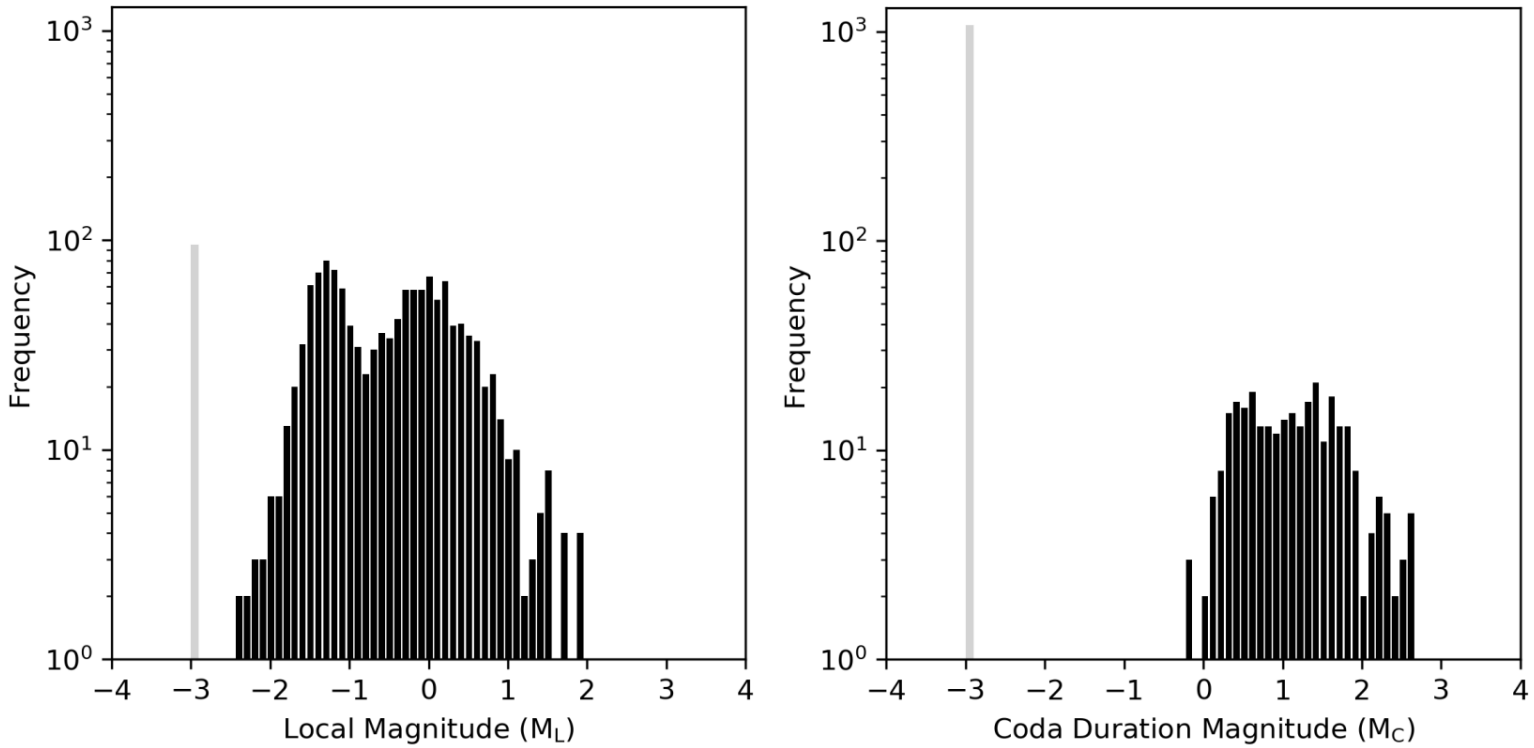

Fig. 3. Magnitude (M_L left and M_C right) distribution for the 1373 events built. The gray bar in each plot represents the number of events for which the magnitude could not be estimated.

MAGNITUDE-BASED DISCRIMINATION

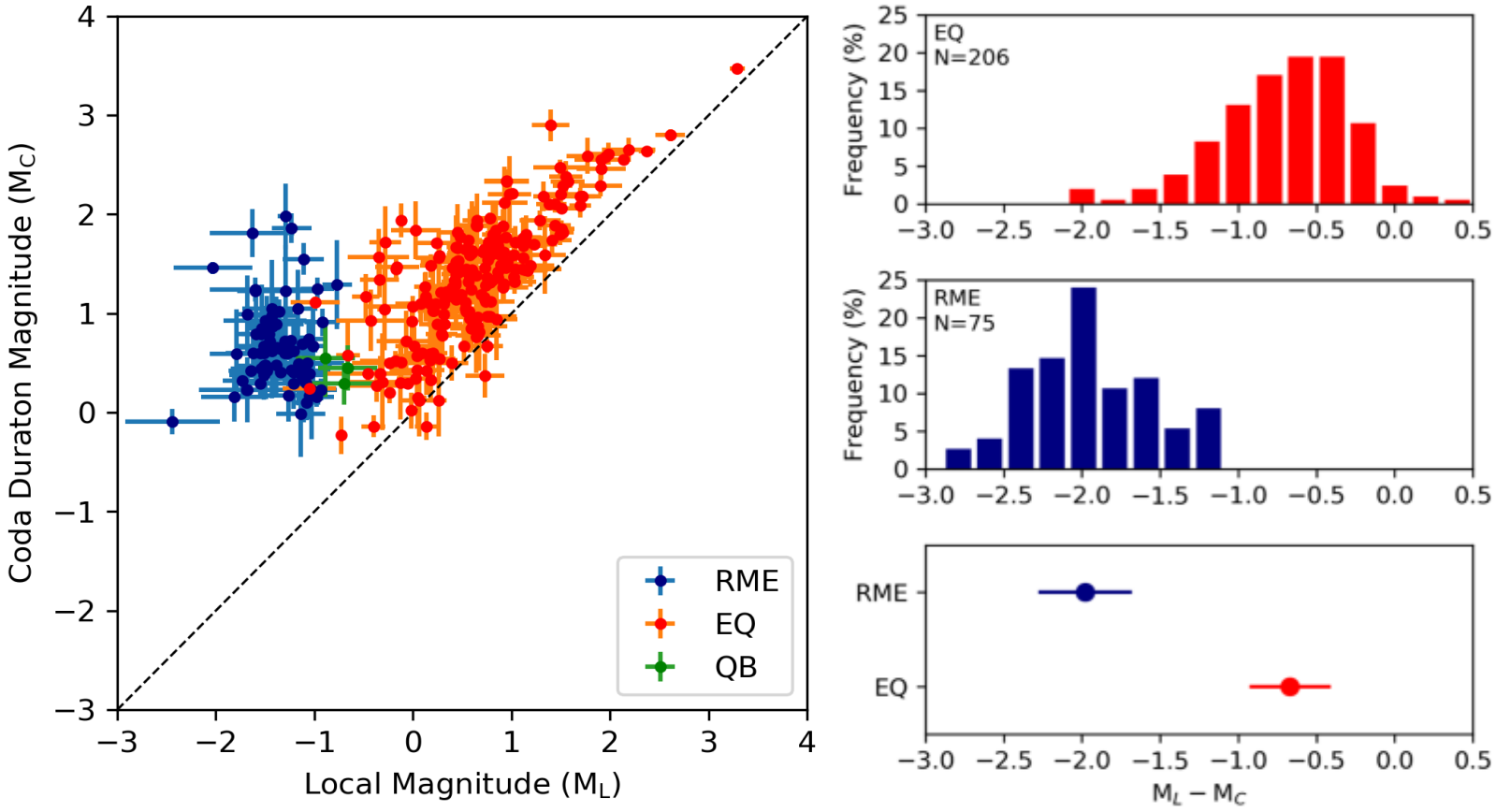

Fig. 4. (Left) M_L–M_C relationship. While data points for EQs plot only slightly above the 1:1 line (dashed line), data points for the mining events (RMEs & QBs) are significantly off that line. This results from enhanced coda for the shallow mining events (Koper et al., 2016). (Right) Distribution and median of M_L–M_C for the EQ and RME populations. Chi-square tests suggest that the two populations are statistically distinct.

MAGNITUDE-BASED DISCRIMINATION

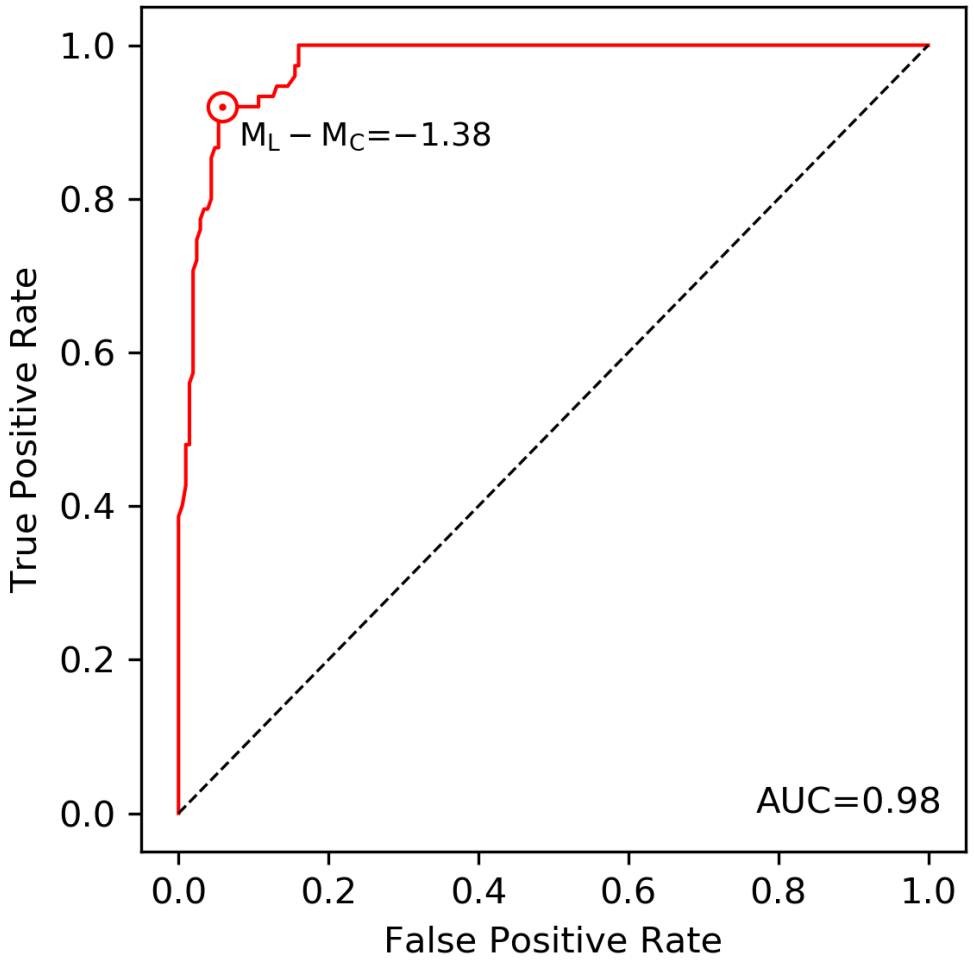

Fig. 5. ROC curve for a binary classifier between RMEs and EQs. The optimum M_L–M_C cutoff associated with the closest point to the ideal classifier is –1.38. The high value for the area under the curve (AUC = 0.98) is a clear indication for a very effective discriminant.

DISCRIMINATION BASED ON FREQUENCY CONTENTS

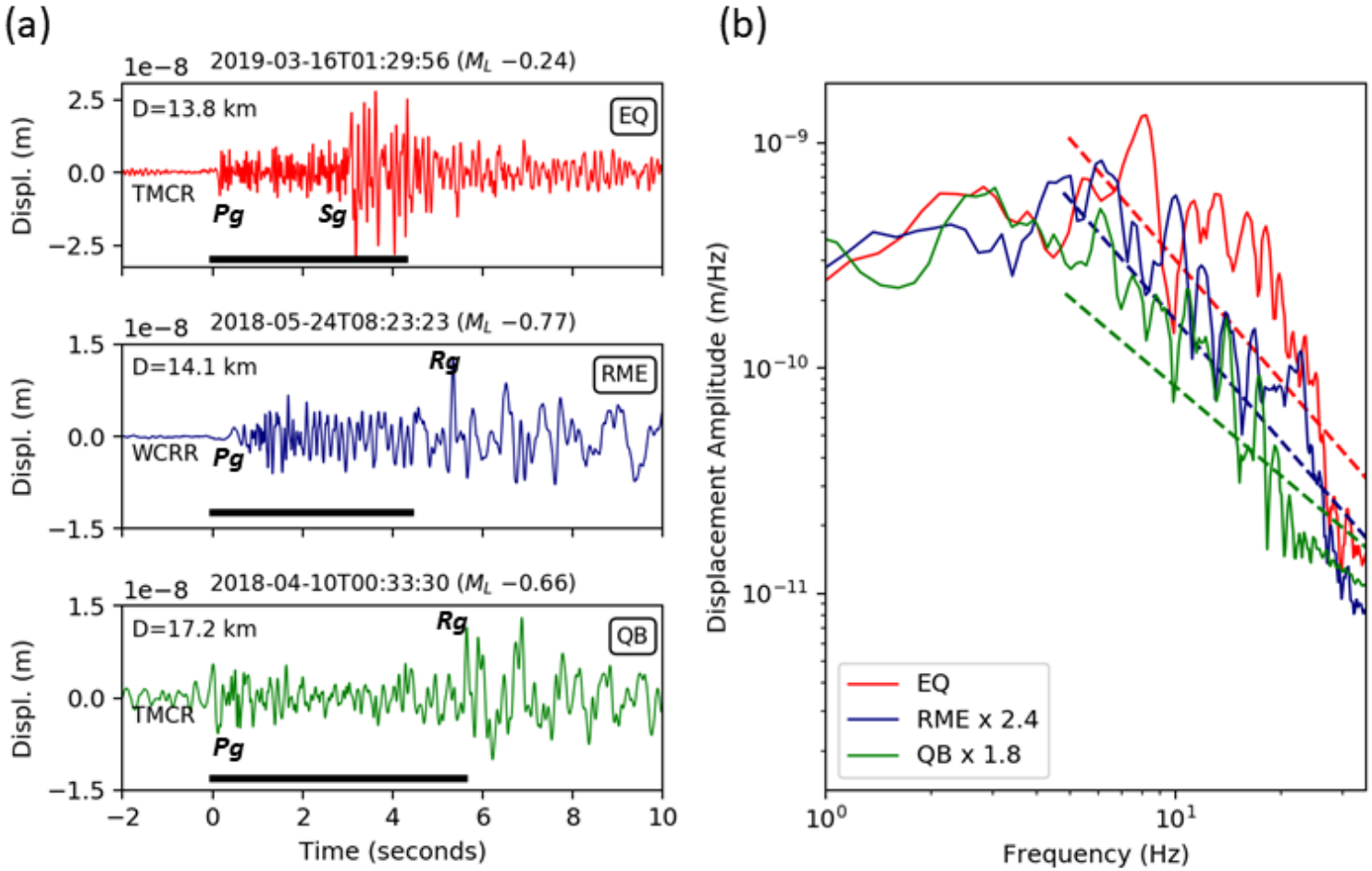

Fig. 6. (a) Example displacement seismograms for an earthquake (EQ), a Redmond Mine event (RME), and a quarry blast (QB). Visible phases are labeled. (b) Spectra for the seismograms shown in (a). The dashed lines are regression lines for the frequency range from 5 to 35 Hz. The slightly steeper fall-off slope for the EQ indicates a lack of high-frequency energy. This constitutes the basis for the discriminant based on low frequency *Sg* to high frequency *Sg* ratio.

DISCRIMINATION BASED ON FREQUENCY CONTENTS

Measurement of Sg Phase Amplitudes

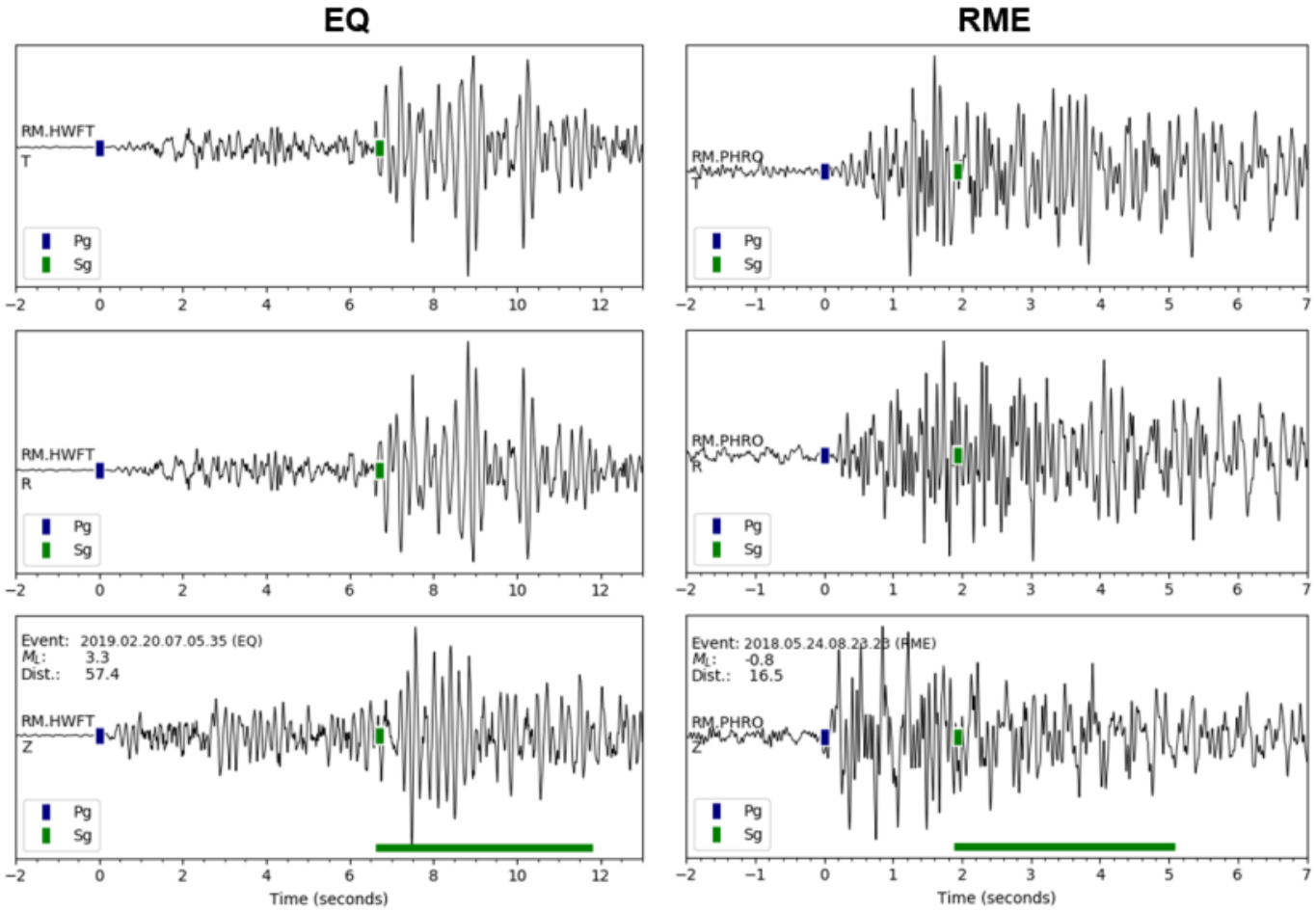

Fig. 7. The root mean square (RMS) of the *Sg* amplitudes are measured in the four frequency bands 5 –10 Hz, 10–15 Hz, 15–20 Hz, and 20–30Hz.

As a result of the Parseval's theorem, the RMS in the time domain is equivalent to the RMS in the frequency domain.

DISCRIMINATION BASED ON FREQUENCY CONTENTS

Separation of Source Excitation, Propagation, and Site Terms

- The recorded amplitude A_{ij} for an event *i* recorded at a station *j* is expressed as in Equation 1.

$$\log A_{ij}(f) = \log EXC_i(f) + \log SITE_j(f) + \log G(r_{ij}, f) \quad (1)$$

$EXC_i(f)$: Source excitation term for source *i*; $SITE_j(f)$: Site term for station *j*;

$G(r_{ij}, f)$: Distance-correction term (combined effect of geometrical spreading and attenuation); r_{ij}: Distance from source *i* to station *j*.

- We parameterized the distance-correction term using a piecewise linear function (Yazd, 1993; Kintner et al., 2020). We defined series of nodes, r_k, in 5-km increment over the source-distance range of 5–100 km ($k = 1, 2, \ldots, 20$).
- Distance-correction term, $G(r_{ij}, f)$, approximated using linear interpolation:

$$G(r_{ij}, f) = G(r_k, f) + \frac{(r_{ij} - r_k)}{(r_{k+1} - r_k)} (G(r_{k+1}, f) - G(r_k, f)) \quad (2)$$

- Linearized equation for an observation at r_{ij} between r_k and r_{k+1}:

$$\log A_{ij}(f) = \log EXC_i(f) + \log SITE_j(f) + q \log G(r_k, f) + p \log G(r_{k+1}, f), \quad (3)$$

$$\text{where } p = \frac{(r_{ij} - r_k)}{(r_{k+1} - r_k)} \text{ and } q = 1 - p$$

- Matrix form: $\boldsymbol{a} = \boldsymbol{Jm}$ (4)
  - $\boldsymbol{a}$: Array of logarithm of amplitude measurements
  - $\boldsymbol{m}$: Array of logarithm of model parameters (source excitation terms, station site terms, and distance-correction terms at nodes 5, 10, 15, …, 100 km)
    - 276 sources, 19 stations, and 20 distance nodes.
- Constraint: For r_k = 5 km, $G(r_k, f) = 1/r_k$ (i.e., only geometrical spreading, no attenuation)
- Least squares solution: $\boldsymbol{m} = (\boldsymbol{J}^T\boldsymbol{J})^{-1}\boldsymbol{J}^T\boldsymbol{a}$ (5)

DISCRIMINATION BASED ON FREQUENCY CONTENTS

Site and Distance-Correction Terms

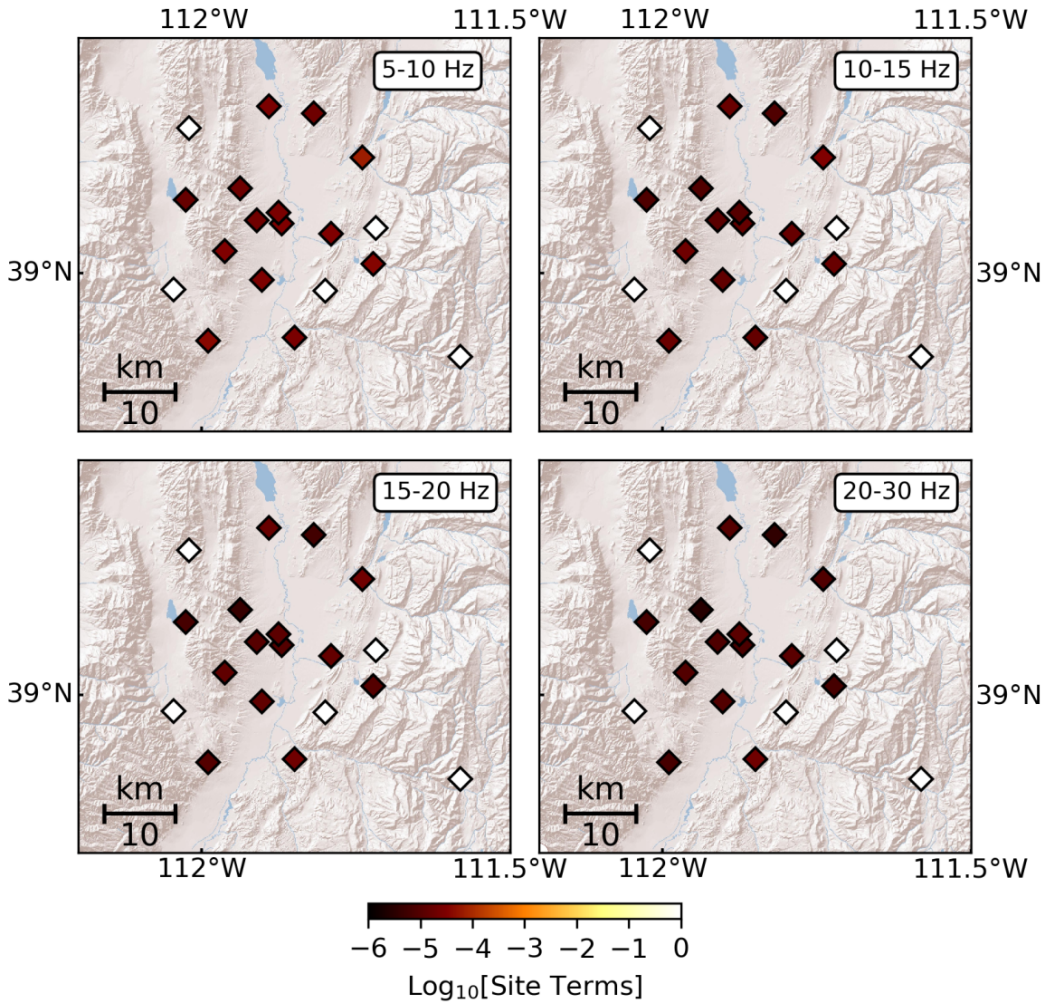

Fig. 8. Site terms for *Sg*. The observed damping at most stations is likely due to locations in basins.

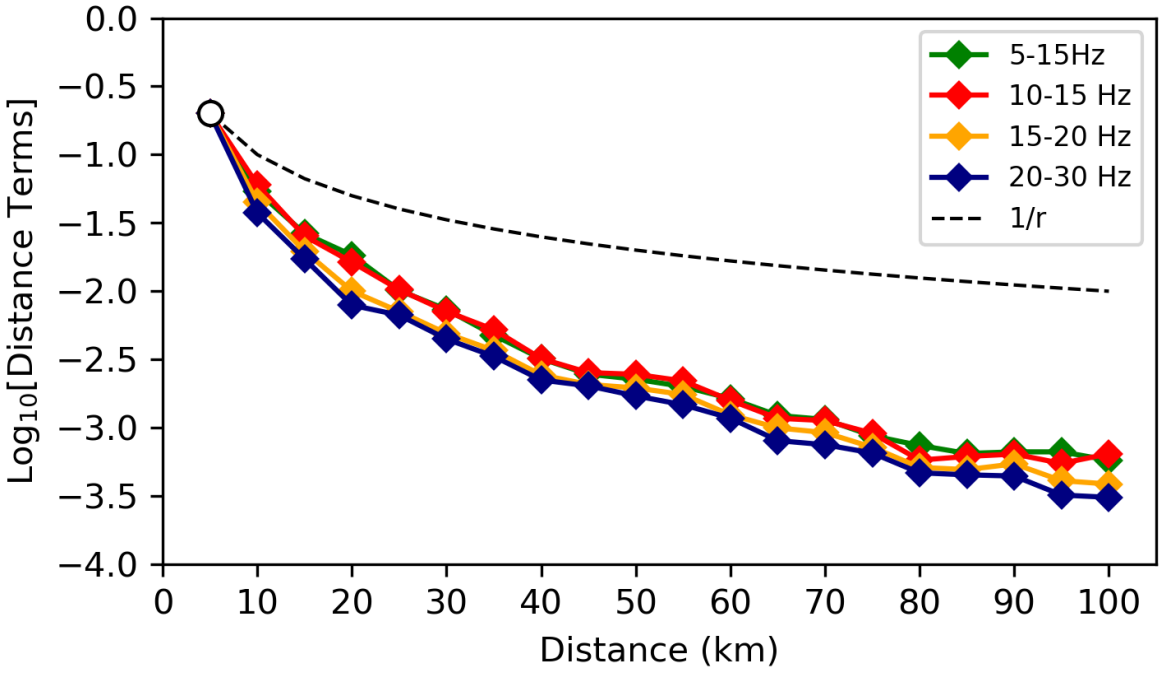

Fig. 9. Distance-correction term as a function of distance. High frequencies are slightly more attenuated than low frequencies.

DISCRIMINATION BASED ON FREQUENCY CONTENTS

Source Terms and Discrimination Based on Low Frequency Sg to High Frequency Sg Ratios

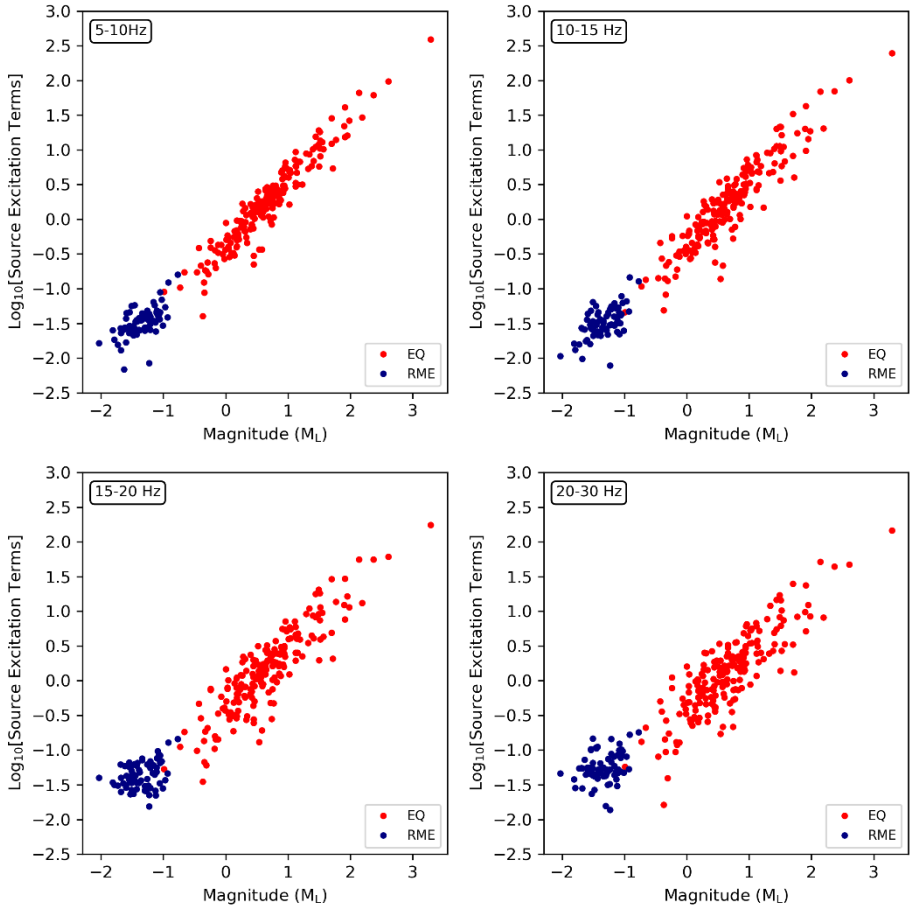

Fig. 10. Source excitation term as a function of magnitude. The degree of scattering of the data points increases with increasing frequency, likely due to decreasing SNR.

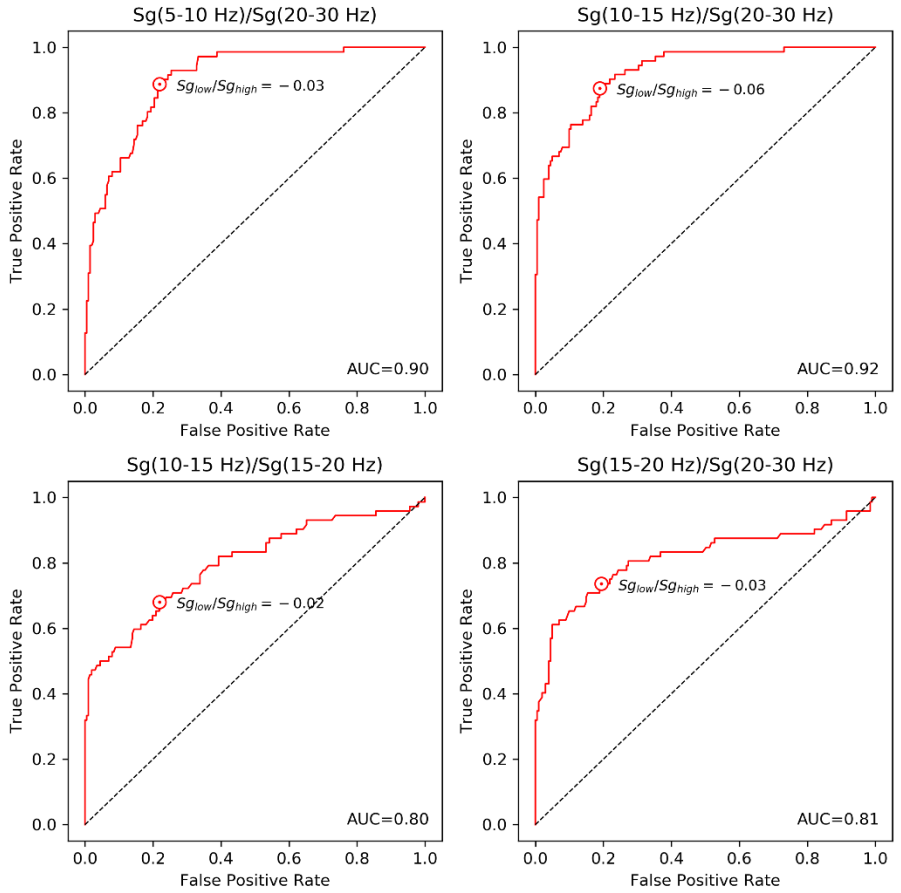

Fig. 11. ROC curve for RMEs vs. EQs. The AUCs range from 0.80 to 0.92, with the highest value associated with $Sg_{[10–15Hz]}/Sg_{[20–30Hz]}$.

DISCRIMINATION BASED ON Pg/Sg PHASE AMPLITUDE RATIOS

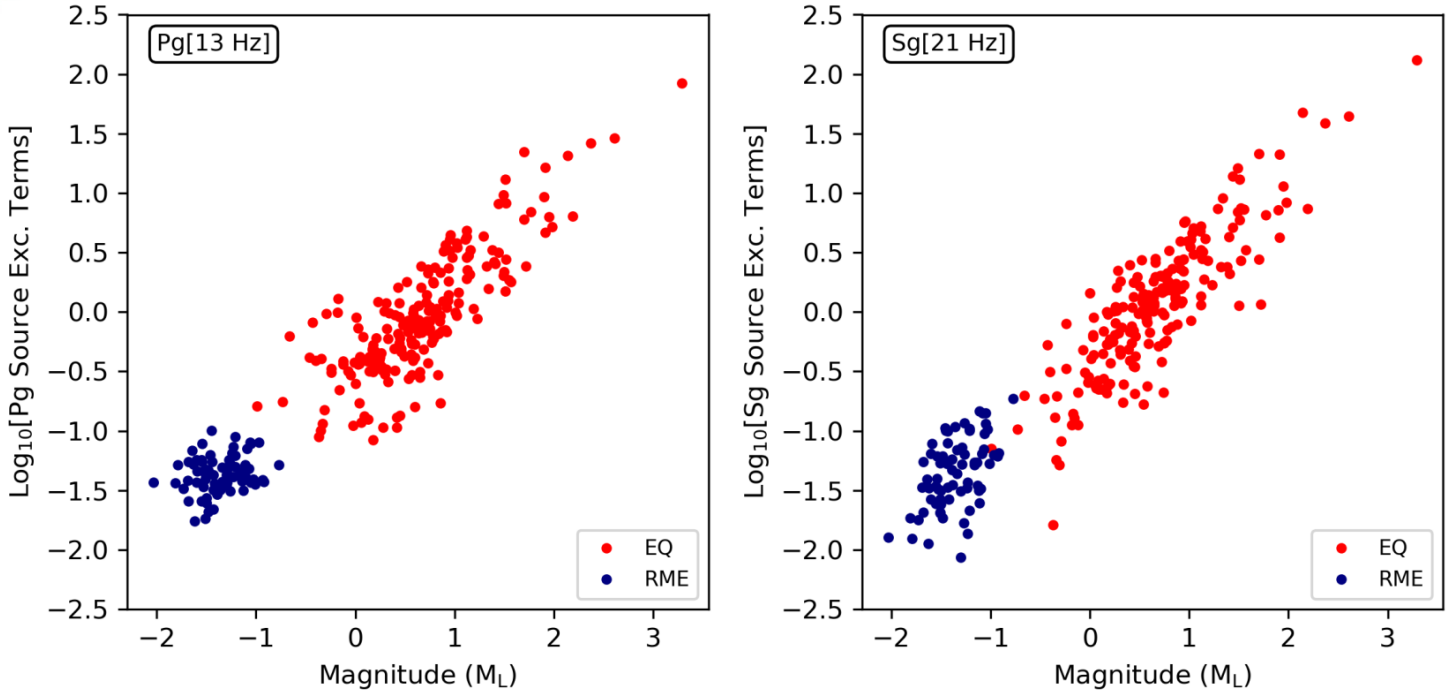

Fig. 12. Source excitation term for $Pg_{[13\ Hz]}$ (left) and $Sg_{[21\ Hz]}$ (right) as a function of magnitude.

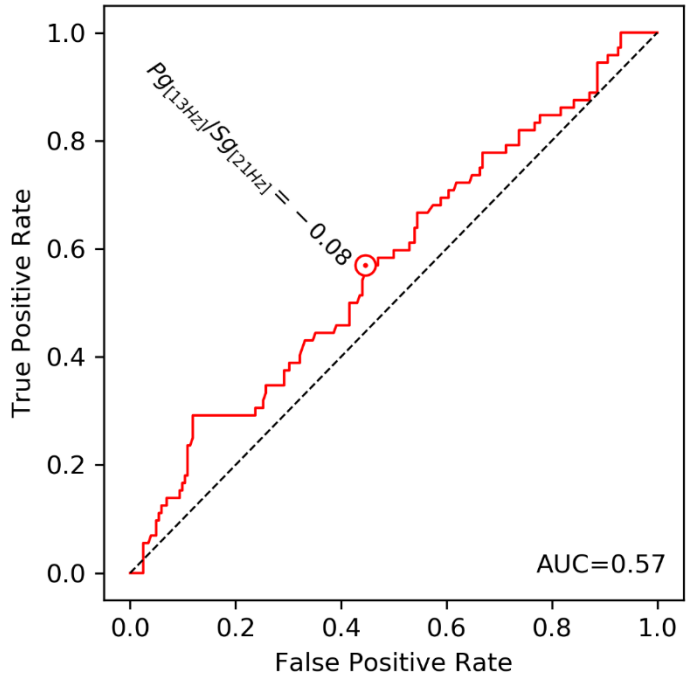

Fig. 13. With an AUC of 0.57, $Pg_{[13\ Hz]}/Sg_{[21\ Hz]}$ is only slightly better than a random classifier.

DEPTH DISCRIMINATION BASED ON Rg/Sg SPECTRAL AMPLITUDE RATIOS

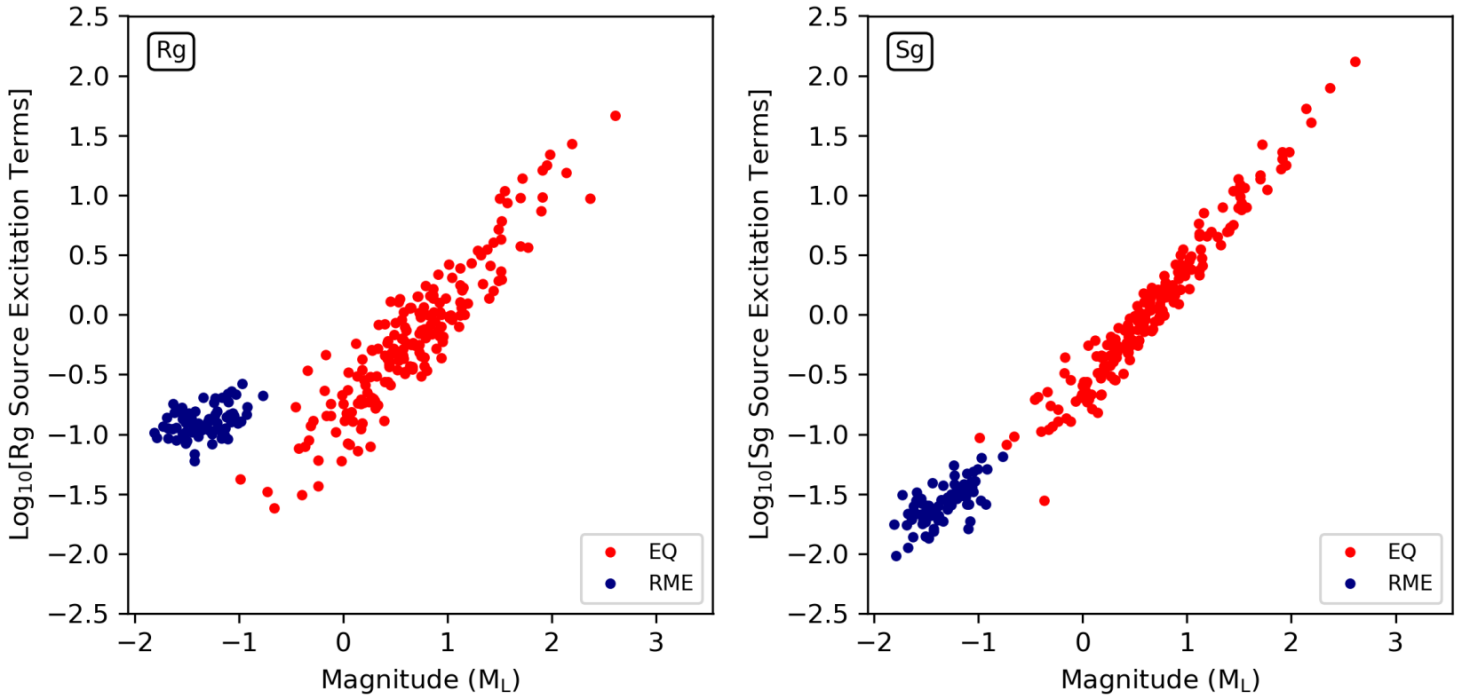

Fig. 14. Source excitation term for $Rg_{[0.5–2\ Hz]}$ (left) and $Sg_{[0.5–8\ Hz]}$ (right) as a function of magnitude. The shallow RMEs excite stronger *Rg* than EQs of similar magnitudes.

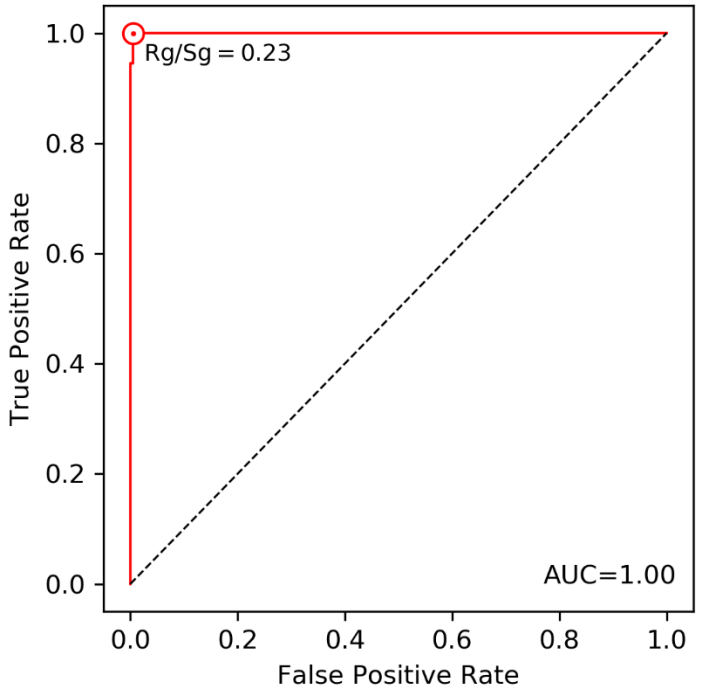

Fig. 15. With an AUC of 1.0, $Rg_{[0.5–2\ Hz]}/Sg_{[0.5–8\ Hz]}$ is an ideal classifier for the RME and EQ groups.

MAHALANOBIS DISTANCE AND LIKELIHOOD OF MISCLASSIFICATION

$$\mathrm{LM} = \frac{1}{\sqrt{2\pi}} \int_{-\infty}^{-\Delta/2} e^{-x^2/2}\, dx$$

	Discriminant			
	$M_L - M_C$	$Sg_{[10–15Hz]}/Sg_{[20–30Hz]}$	Pg/Sg	$Rg_{[0.5–2\ Hz]}/Sg_{[0.5–8\ Hz]}$
Mahalanobis Distance (Δ^2)	4.0	1.95	0.03	11.8
Minimum Likelihood of Misclassification (LM in %)	16.0	24.3	46.4	4.3

Table 1: Based on LM values, from all the fours classifiers, *Rg/Sg* is the best for the population of RMEs vs. EQs.

MULTIVARIATE DISCRIMINATION

GOAL: Improve discriminant power by combining 2 or more (uncorrelated) discriminants

Combination	LM Improvement (%)
$M_L - M_C$ and *low Sg/high Sg*	-0.2
$M_L - M_C$ and *Rg/Sg*	4
$M_L - M_C$ and *Pg/Sg*	-2.7
low Sg/high Sg and *Rg /Sg*	4.1
low Sg/high Sg and *Pg/Sg*	-9.4
Rg/Sg and Pg/Sg	3.9

Table 2: LM improvements are relative to the best performing single discriminant, *Rg/Sg.*

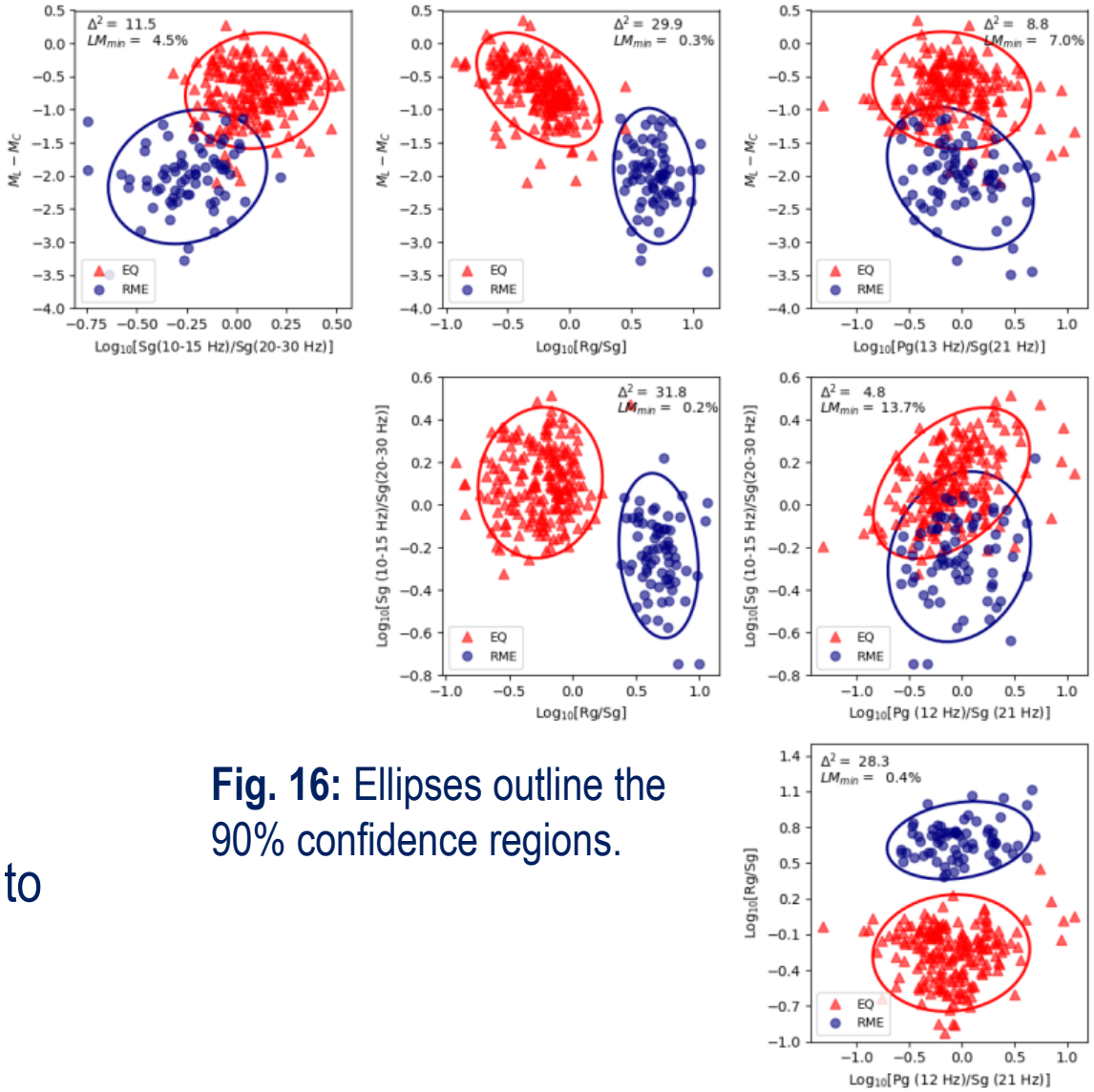

Fig. 16: Ellipses outline the 90% confidence regions.

MULTIVARIATE DISCRIMINATION

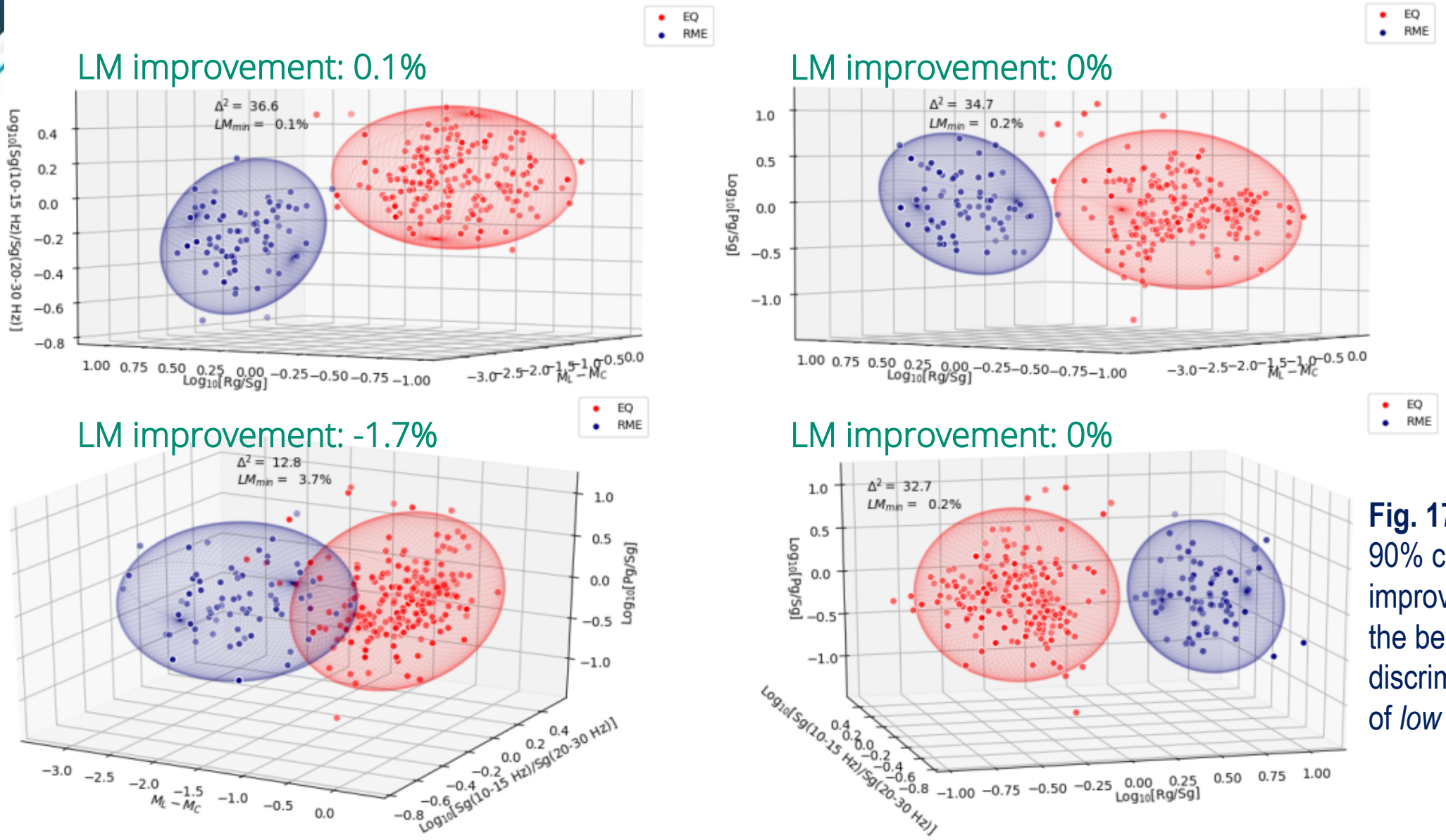

Fig. 17: Ellipsoids outline the 90% confidence regions. LM improvements are relative to the best performing bivariate discriminant, the combination of *low Sg/high Sg* and *Rg/Sg*.

Conclusions

- We tested and designed several discriminants to separate the population of mining blasts from the group of earthquakes recorded at local distances. The discriminants consist of $M_L - M_C$, low frequency *Sg to* high frequency *Sg ratio (low Sg/high Sg)*, *Pg/Sg, and Rg/Sg,* and different combinations of 2 or more of these discriminants.

- While the areas under the receiver operating characteristic curve (AUC) of 0.92–1.0 for $M_L - M_C$, *low Sg/high Sg*, and *Rg/Sg*, indicate that these discriminants are very effective, the AUC of only 0.57 suggests that *Pg/Sg* is only slightly better than a random classifier.

- Among the classifiers, *Rg/Sg*, which is a depth discriminant, shows the lowest likelihood of misclassification (LM = 4.3%) for the populations.

- To improve the discriminant power, we combined 2 and more of the discriminants by performing multivariate discriminant analyses. For the bivariate classifier, the combination of *Rg/Sg* with *low Sg/high Sg* provides the largest improvement (4.1% or LM = 0.2%) over the best single discriminant, while for the best performing trivariate classifier this improvement is 4.2% (LM = 0.1%).